The Astrophysical Journal Supplement Series, 251:12 (12pp), 2020 November https://doi.org/10.3847/1538-4365/abba28

Deuterated Polycyclic Aromatic Hydrocarbons in the Interstellar Medium: The C–D Band Strengths of Monodeuterated Species

X. J. Yang[1,2], Aigen Li[2], and R. Glaser[3]
[1] Key Laboratory of Stellar and Interstellar Physics and Department of Physics, Xiangtan University, 411105 Xiangtan, Hunan Province, People's Republic of China xjyang@xtu.edu.cn
[2] Department of Physics and Astronomy, University of Missouri, Columbia, MO 65211, USA; lia@missouri.edu
[3] Department of Chemistry, University of Missouri, Columbia, MO 65211, USA; glaserr@missouri.edu
Received 2020 July 28; revised 2020 August 29; accepted 2020 September 17; published 2020 November 9

Abstract

Deuterium (D) is one of the light elements created in the Big Bang. As the Galaxy evolves, the D/H abundance in the interstellar medium (ISM) decreases from its primordial value due to astration. However, the observed gas-phase D/H abundances of some sightlines in the local Galactic ISM are substantially lower than the expected reduction by astration. The missing D could have been depleted onto polycyclic aromatic hydrocarbon (PAH) molecules which are ubiquitous and abundant in interstellar regions. To quantitatively explore the hypothesis of PAHs as a possible reservoir of interstellar D, we quantum-chemically compute the infrared vibrational spectra of monodeuterated PAHs and their cations. We find that, as expected, when H in PAHs is replaced by D, the C–H stretching and bending modes at 3.3, 8.6, and 11.3 μm shift to longer wavelengths at $\sim$4.4, 11.4, and 15.4 μm, respectively, by a factor of $\sim\sqrt{13/7}$, the difference in reduced mass between the C–H and C–D oscillators. From the computed spectra we derive the mean intrinsic band strengths of the 3.3 μm C–H stretch and 4.4 μm C–D stretch to be $\langle A_{3.3}\rangle \approx 13.2$ km mol^{-1} and $\langle A_{4.4}\rangle \approx 7.3$ km mol^{-1} for neutral deuterated PAHs which would dominate the interstellar emission at 3.3 and 4.4 μm. By comparing the computationally derived mean band-strength ratio of $\langle A_{4.4}/A_{3.3}\rangle \approx 0.56$ for neutral PAHs with the mean ratio of the observed intensities of $\langle I_{4.4}/I_{3.3}\rangle \approx 0.019$, we find that the degree of deuteration (i.e., the fraction of peripheral atoms attached to C atoms in the form of D) is $\sim$2.4%, corresponding to a D enrichment of a factor of $\sim$1200 with respect to the interstellar D/H abundance.

Unified Astronomy Thesaurus concepts: Polycyclic aromatic hydrocarbons (1280); Interstellar line emission (844); Line intensities (2084); Astrochemistry (75); Interstellar molecules (849)

1. Introduction

Deuterium (D) is a primordial element that was only made during the first minutes after the Big Bang (Epstein et al. 1976). The primordial D/H abundance ($[D/H]_{prim}$) established by Big Bang nucleosynthesis (BBN) is sensitive to the cosmological parameters (e.g., the baryon closure parameter, Ω_b, and the Hubble constant, h; see Boesgaard & Steigman 1985). D could be easily destroyed by nuclear fusion in stellar interiors, a process known as "astration." Through astration, D is converted to ^{3}He, ^{4}He, and heavier elements, and as a result, the cosmic D/H abundance is expected to decrease monotonically with the chemical evolution of the Galaxy (Mazzitelli & Moretti 1980). Therefore, the interstellar D/H abundance in the present epoch is directly related to the primordial nucleosynthesis and the subsequent Galactic chemical evolution.

To reliably measure $[D/H]_{prim}$, one often relies on metal-poor quasar absorption line systems or damped Lyα absorption systems which are compositionally as "pristine" as possible and thus still retain a primordial composition of D. To date, the primordial D/H abundance has been reliably determined to be $[D/H]_{prim} \approx 25$–28 ppm, based on high-precision measurements of the column densities of D I and H I of seven such systems (e.g., see Cooke et al. 2018; Zavarygin et al. 2018). Alternatively, one can also infer $[D/H]_{prim}$ from η, the ratio of the baryons to photons, which is simply related to $\Omega_b h^2$ (Burles et al. 2001). In the standard BBN model, η is the single parameter that predicts the primordial light element abundances including $[D/H]_{prim}$ (e.g., see Boesgaard & Steigman 1985). Using the Ω_b and h parameters derived from observations of the cosmic microwave background, Spergel et al. (2003), Coc et al. (2004), and Sánchez et al. (2006) found $[D/H]_{prim} \approx 26$ ppm, which is in close agreement with that measured from the pristine quasar absorption systems. As the Galaxy evolves, D is "astrated" and the D/H abundance in the interstellar medium (ISM) decreases from its primordial value. This is because D is destroyed in the Galaxy as gas is cycled through stars. On the other hand, infall to the disk of the Galaxy of less processed or astrated gas, which is D-rich and metal-poor, from the intergalactic medium and small galaxies captured by the Milky Way, would raise the interstellar D/H abundance closer to the primordial value. Careful studies of the competition between stellar destruction and infall derived the present day interstellar D/H abundance to be $[D/H]_{ISM} \gtrsim 20 \pm 1$ ppm (e.g., see Prodanović et al. 2010).

Accurate measurements of the gas-phase D/H abundance have been made for more than 40 interstellar lines of sight, based on the high-resolution ultraviolet (UV) absorption spectra of H I and D I, obtained with the Copernicus satellite, the International Ultraviolet Explorer (IUE) satellite, and the Far Ultraviolet Spectroscopic Explorer (FUSE) satellite, as well as the Goddard High Resolution Spectrometer and Space Telescope Imaging Spectrograph instruments on board the Hubble Space Telescope, and the Interstellar Medium Absorption Profile Spectrograph on the ORFEUS-SPAS II mission (see Wood et al. 2004; Draine 2006; Linsky et al. 2006 and references therein). These measurements revealed an unexplained mystery: the gas-phase D/H abundance varies significantly by a factor of $\sim$4 from one sightline to another within a few hundred parsecs of the Sun (see, e.g., Moos et al. 2002; Steigman 2003; Wood et al. 2004; Hébrard et al. 2005).

It had been suggested that the observed regional variations in $[D/H]_{gas}$ could be due to the regional variations in astration. The gas returned to the ISM from stars is expected to be nearly devoid of D, as the D is converted to ^{3}He during the pre-main-sequence evolution of stars with a mass of $M \lesssim 5\,M_{\odot}$ (Mazzitelli & Moretti 1980). As a result, the D/H abundance in the ISM is an indicator of the fraction of the baryons now in the ISM that have passed through a star. If different sightlines have different star formation histories so that the interstellar matter has been cycled through stars to different degrees, then the D astration will be different for different sightlines: for sightlines with a stronger star formation activity, more D will be destroyed and therefore one would expect a smaller $[D/H]_{gas}$. However, it is difficult to imagine how regions separated by only a few hundred parsecs can have had extremely different star formation histories. It is also difficult to imagine why turbulent diffusion has not homogenized the ISM in regions situated just a few hundred parsecs apart. Turbulent mixing is expected to be effective at mixing gas over length scales of hundreds of parsecs on 10^9 yr timescales and one would expect that the elemental abundances in the gas have been homogenized (see Draine 2006).

As early as 1982, it had been suggested that D might be depleted from the gas phase and sequestered in dust grains (Jura 1982). Allamandola et al. (1987) analyzed the carbonaceous matter in interplanetary dust particles and meteorites and found that they are D enriched (i.e., the D/H ratios are considerably greater than the canonical interstellar D/H ratio). Sandford et al. (2001) have revealed several processes that could lead to D enrichment in carbonaceous material (also see Wiersma et al. 2020). Draine (2004) argued that carbonaceous interstellar grains could incorporate enough D atoms to substantially reduce the D abundance in the gas phase and the observed variations in the gas-phase $[D/H]_{gas}$ abundance could be attributed to variations from one sightline to another in the fraction of the D sequestered in dust grains.

As the smallest carbonaceous grains, polycyclic aromatic hydrocarbon (PAH) molecules could be a major reservoir of interstellar D (Draine 2004). PAHs are abundant and widespread throughout the universe, as revealed by their distinctive set of infrared (IR) emission bands at 3.3, 6.2, 7.7, 8.6, 11.3, and 12.7 μm, which are characteristic of their vibrational modes (see Allamandola et al. 1985; Bernstein et al. 2017; Li 2020). PAHs of intermediate size are expected to become enriched in D in space through the selective loss of H during photodissociation events. Since the aromatic C–D bond zero-point energy is about 30% lower than that of the C–H bond, H loss is favored over D loss. For PAHs in typical interstellar environments, the C–D bond rupture rate is $\sim$3 times lower than that of the C–H bond; the PAH D/H ratio might therefore be substantially larger than the interstellar abundance of $[D/H]_{ISM} \sim 2 \times 10^{-5}$ (Allamandola et al. 1989). Draine (2006) showed that collisions of D with PAH cations, and collisions of D^+ with PAHs, are expected to result in the incorporation of D into PAHs, with the rate of such collisions sufficiently rapid to deplete D from the gas on timescales of $\sim$2 Myr in cool diffuse clouds.

PAHs show three emission features associated with vibrations of the C–H bond: the C–H stretch at 3.3 μm, the in-plane C–H bending at 8.6 μm, and the out-of-plane (oop) C–H bending at 11.3 μm. The stretching and bending modes can be approximated as harmonic oscillators. If a peripheral H atom is replaced by D, the reduced mass of the C–H oscillator will increase by a factor of 13/7, and the wavelength (λ) will be increased by a factor of $\sim\sqrt{13/7}$. Therefore, deuterated PAHs will emit at $\sim$4.4 μm (C–D stretching), $\sim$11.7 μm (C–D in-plane bending), and $\sim$15.4 μm (C–D oop bending). While the 11.7 μm C–D feature would be confused with the C–H oop bending modes at $\sim$11.3 μm and the 15.4 μm C–D feature falls in a region where other PAH features (i.e., the C–C–C skeleton modes) are present, the 4.4 μm C–D feature appears to be the best probe of the deuteration of interstellar PAHs (see Hudgins et al. 1994, 2004; Bauschlicher et al. 1997; Draine 2006).

Observationally, the C–D emission feature at $\sim$4.4 μm of interstellar deuterated PAHs is often much weaker than the C–H features at 3.3 μm (e.g., see Peeters et al. 2004; Onaka et al. 2014; Doney et al. 2016). The detection and identification of the feature as due to C–D are hampered by its small intensity which would put it at the limit of modern observational techniques, including the Short Wavelength Spectrometer (SWS) on board the Infrared Space Observatory (ISO) and the Infrared Camera (IRC) on board AKARI.[4] This will change with the launch of James Webb Space Telescope (JWST). The Near Infrared Spectrograph instrument on JWST will cover the wavelength range of the C–H and C–D stretches of deuterated PAHs with high spectral resolution and unprecedented sensitivity. JWST's unique high-sensitivity and high-resolution near-IR capabilities will open up an IR window unexplored by Spitzer and unmatched by ISO observations and thus will place the detection of deuterated PAHs on firm ground and enable far more detailed band analysis than previously possible, and therefore will allow us to quantitatively test the D depletion hypothesis as a viable explanation of the observed regional variations of the gas-phase D/H abundance by accurately determining the deuteration degree of interstellar PAHs.

To this end, one requires a prerequisite knowledge of the intrinsic strengths of the C–D bands of deuterated PAHs. This motivates us to compute the IR spectra of astrophysically relevant deuterated neutral and ionized PAHs. Our goal is to computationally determine the intrinsic strengths of the C–D bands. To our knowledge, laboratory IR spectra have only been obtained from a number of matrix-isolated perdeuterated PAHs (i.e., PAHs in which all of the peripheral H atoms have been replaced by D atoms; Hudgins et al. 1994; Bauschlicher et al. 1997). However, as mentioned earlier, while the interstellar PAH population is expected to be enriched in D over the canonical interstellar D/H ratio, it is highly unlikely that they would be fully deuterated (see Hudgins et al. 2004). Moreover, the absolute C–D band intensities have not been measured for those matrix-isolated perdeuterated PAHs (Hudgins et al. 1994; Bauschlicher et al. 1997). On the other hand, quantum chemical computations have so far been limited to perdeuterated PAHs (Bauschlicher et al. 1997), D-enriched superhydrogenated PAHs (i.e., PAHs with extra H and D atoms attached to some of their peripheral C atoms; Hudgins et al. 2004), deuteronated PAHs (i.e., PAHs to which a deuteron is added; Buragohain et al. 2015), deuterated ovalene (Buragohain et al. 2016), and PAHs with D-substituted aliphatic side groups (Buragohain et al. 2020). In this work, we will systematically calculate the IR spectra of all the isomers of a large range of singly deuterated PAH species and thoroughly explore the effects of deuteration on their IR spectra. Multideuterated PAHs will be the focus of a separate companion paper. We will obtain the C–D band intensities of deuterated PAHs and apply them to astronomical data to derive the deuteration degrees—the fractions of peripheral (H and D) atoms attached to C atoms in the form of D—of interstellar PAHs.

[4] The Infrared Spectrograph on board Spitzer only operates longward of $\sim$5.2 μm.

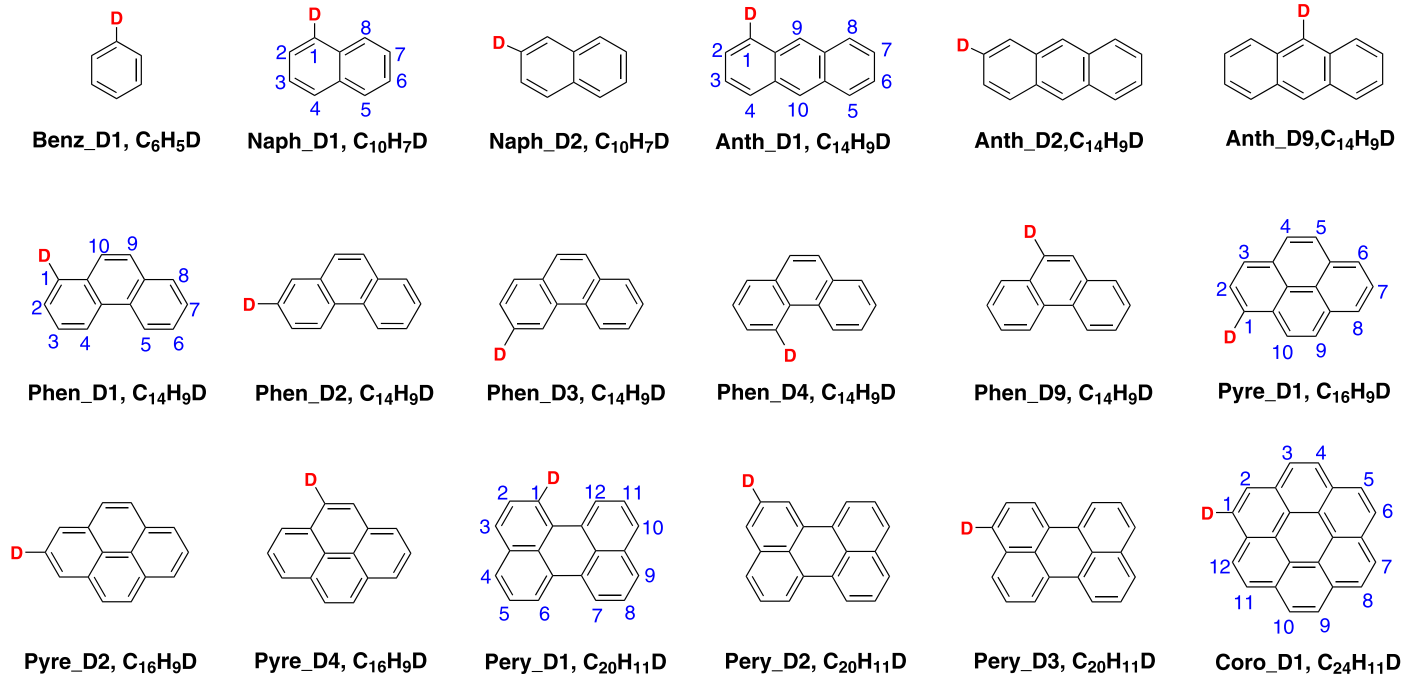

Figure 1. Structures of monodeuterated PAHs. We refer to a monodeuterated species by the abbreviation of the first four letters of the name of its parent molecule followed by the position where the D atom is attached (e.g., Anth_D2 refers to anthracene with the D atom attached at position 2).

This paper is organized as follows. In Section 2 we briefly describe the computational methods and the selected target molecules. The computed IR vibrational spectra and the derived intrinsic C–D band strengths are reported in Section 3. In Section 4 we apply the derived band strengths to ISO/SWS and AKARI/IRC data to determine the deuteration degrees of interstellar PAHs. Finally, we summarize our major results in Section 5.

2. Computational Methods and Target Molecules

We use the Gaussian09 software (Frisch et al. 2009) to calculate the IR vibrational spectra for a series of deuterated PAH molecules and cations of various numbers of carbon atoms (N_C). Our target molecules include all the possible singly deuterated isomers of an ensemble of seven PAH species in both neutral and cationic forms (see Figure 1).[5] To facilitate comparison with experimental results, we will also calculate four perdeuterated species (see Figure 2): perdeuterated benzene (C_6D_6), naphthalene ($C_{10}D_8$), phenanthrene ($C_{14}D_{10}$), and pyrene ($C_{16}D_{10}$). We note here that in our target molecules, all the D atoms are attached to the aromatic C atoms, therefore our calculations will mainly explore the vibrational properties of aromatic C–D bonds.

We will refer to monodeuterated species by the abbreviation of the first four letters of the names of their parental PAH molecules followed by the position where the D atom is attached (e.g., Naph_D2 refers to naphthalene with the D atom attached at position 2).

We employ the hybrid density functional theoretical method (B3LYP) at the 6–311+G** level, which gives sufficient calculational accuracies with operable computer time (see Yang et al. 2017 and references therein). The standard scaling is applied to the frequencies by employing a scale factor of ∼0.9688 (Borowski 2012).

[5] Here we focus on small PAHs of $N_C \lesssim 24$, since D enrichment in PAHs of $N_C \gtrsim 40$ is not expected: these larger PAHs have a sufficiently large number of internal degrees of freedom to accommodate the maximum energy of typical UV photons without subsequent photolytic bond cleavage occurring (Hudgins et al. 2004).

3. Results

3.1. Perdeuterated PAHs

We first show our calculational results for perdeuterated PAHs, because these are the ones with experimental data are available for comparison. Our target molecules are perdeuterated benzene (Benz_6D), naphthalene (Naph_8D), phenanthrene (Phen_10D) and pyrene (Pyre_10D). The experimental spectrum of Benz_6D is taken from the National Institute of Standards and Technology (NIST) webbook[6], while the others are taken from Bauschlicher et al. (1997). Since the experimental data do not have information for the band intensities, we will only compare the relative intensities with our calculations.

Figure 3(a) shows the computed IR spectrum of Benz_6D (red line), expressed as the molar extinction coefficient $\varepsilon_{\tilde{\nu}}$ normalized to its peak value $\varepsilon_{\tilde{\nu},\mathrm{max}}$, where $\tilde{\nu} \equiv \lambda^{-1}$ is the wavenumber.[7] The experimental spectrum of Benz_6D taken

[6] https://webbook.nist.gov/chemistry/

[7] The molar extinction coefficient $\varepsilon_{\tilde{\nu}}$ measures how strongly a chemical species or substance absorbs light at a particular wavelength. It is an intrinsic property of chemical species that is dependent upon their chemical composition and structure. The absorption cross section per molecule $C_{\mathrm{abs}}(\lambda)$ relates to $\varepsilon_{\tilde{\nu}}$ through

$$\frac{C_{\mathrm{abs}}(\lambda)}{\mathrm{cm^2\ molecule^{-1}}} = \frac{1}{6.02 \times 10^{16}} \times \frac{\varepsilon_{\tilde{\nu}}}{\mathrm{L\ mol^{-1}\ cm^{-1}}}. \quad (1)$$

The band strength A_λ relates to $\varepsilon_{\tilde{\nu}}$ and $C_{\mathrm{abs}}(\lambda)$ through

$$\begin{aligned}\frac{A_\lambda}{\mathrm{km\ mol^{-1}}} &= 100 \times \int \frac{\varepsilon_{\tilde{\nu}}}{\mathrm{L\ mol^{-1}\ cm^{-1}}}\, d\tilde{\nu} \\ &= 6.02 \times 10^{18} \times \int \frac{C_{\mathrm{abs}}(\lambda)}{\mathrm{cm^2\ molecule^{-1}}}\, d\tilde{\nu}, \quad (2)\end{aligned}$$

where the integrations are performed over the band.

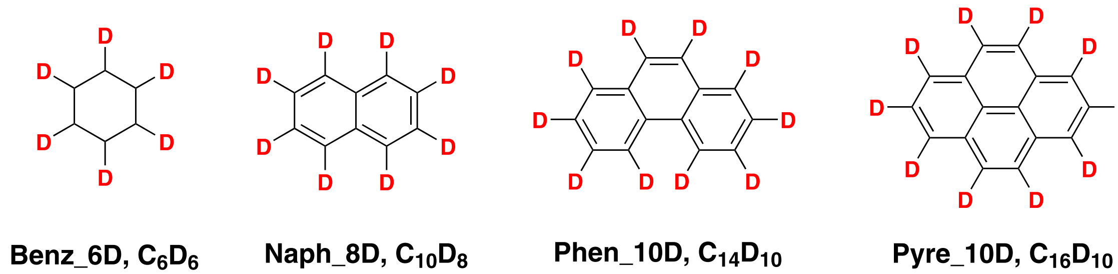

Figure 2. Structures of fully deuterated (i.e., perdeuterated) PAHs.

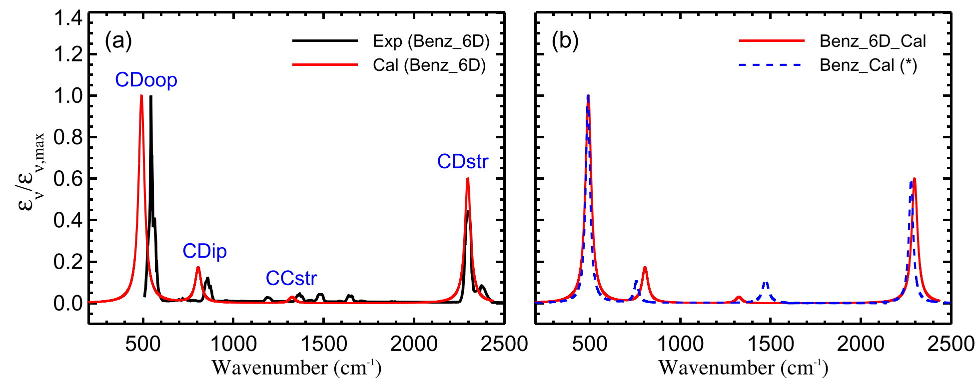

Figure 3. (a) Comparison of the experimental spectrum of fully deuterated (i.e., perdeuterated) benzene taken from the NIST webbook (black solid line) with that computed from B3LYP/6-311+G** (red solid line). The C–D bands are labeled as CDstr (for the C–D stretching bands), CDip (for the C–D in-plane bending bands), and CDoop (for the C–D oop bending bands). Also labeled (as CCstr) is the C–C stretching bands. To better match the experimental spectrum, the calculated frequencies are scaled with a factor of 0.9748 (instead of the canonical scale factor of 0.9688) and a line width of 20 cm^{-1} is assigned. To facilitate comparison, we normalize the experimental and computational spectra (in terms of molar extinction coefficient $\varepsilon_{\tilde{\nu}}$) to their maxima ($\varepsilon_{\tilde{\nu},\max}$) since the experimental spectrum does not have information for the (absolute) intensities. (b) Comparison of the computational spectrum of fully deuterated benzene (red solid line) with that of pure benzene (blue dashed line). For pure benzene, the C–H bands originally at $\sim$663 cm^{-1} (oop bending), 1026 cm^{-1} (in-plane bending), and 3085 cm^{-1} (stretching) are scaled with a factor of $\sqrt{7/13}$ while the features related to the benzene ring at $\sim$1463 cm^{-1} stay intact.

from the NIST webbook is also shown in Figure 4(a) (black line). By applying a single scaling factor of 0.9748 (instead of the canonical scaling factor of 0.9688) for the calculated frequencies, the computational C–D stretching feature closely matches that of the experimental spectrum, while the other features at smaller wavenumbers seems to require a somewhat larger scaling factor.

Benz_6D is highly symmetric, and its vibrational modes are highly degenerate, just like benzene. Its IR spectrum shows only four peaks, which is quite similar to benzene. The only difference is that the C–D bond has a larger reduced mass, by a factor of 13/7, therefore the vibrational modes related to the C–D bond will appear at a smaller wavenumber, by a factor of $\sim\sqrt{7/13}$. To illustrate this, we show in Figure 3(b) the IR spectrum of benzene calculated with the same method (blue dashed line). We scale the three features related to the C–H vibrations at wavenumbers of $\sim$663 cm^{-1} (C–H oop bending), 1026 cm^{-1} (C–H in-plane bending), and 3085 cm^{-1} (C–H stretching) with a factor of $\sqrt{7/13}$, while keeping the benzene-ring-related features at $\sim$1463 cm^{-1} intact. Figure 3(b) clearly demonstrates that after scaling, the frequencies of the C–D and C–H stretching and oop bending features match quite well with each other, while the C–D in-plane bending features of perdeuterated PAHs are blueshifted and relatively weaker. Meanwhile, when the H atoms are replaced with D, the C–C stretching features at $\sim$1460 cm^{-1} are redshifted and seriously depressed.

Figure 4 shows the calculated and experimental spectra of Benz_6D (a), Naph_8D (b), Phen_10D (c), and Pyre_10D (d) in the frequency range of 2200–2400 cm^{-1}. Here we focus on the C–D stretching bands of Naph_8D, Phen_10D, and Pyre_10D in Figure 4(a), which is a zoomed-in view of Figure 3(a). The experimental spectra basically show two major peaks and several satellite features. The calculated frequencies match the experimental ones quite well after scaling with a factor of 0.9688 (0.9748 for Benz_6D) and applying a line width of 4 cm^{-1} (20 cm^{-1} for Benz_6D). Again, since only the relative intensities were measured for the C–D bands from the experimental spectra (Bauschlicher et al. 1997), we compare the relative band intensities of the experimental spectra with those of our calculations. As tabulated in Table 1, the relative intensities are quite consistent with each other. In view of the close match between our calculations and the experimental data, we conclude that our calculations provide reliable frequencies and relative intensities for the C–D vibrational modes.

3.2. Monodeuterated PAHs

Considering the relatively low overall cosmic D/H abundance (see Section 1), it is reasonable to assume that singly deuterated PAHs play a more important role in astrophysics. Meanwhile, we focus on the 3.3 μm C–H stretch and the 4.4 μm C–D stretch, which mainly originate from small PAH molecules of $\sim$20–30 C atoms (see Figure 7 of Draine & Li 2007). Therefore, we calculate the IR spectra of seven small monodeuterated PAH species and their cations: *d*-benzene (C_6H_5D), *d*-naphthalene ($C_{10}H_7D$), *d*-anthracene ($C_{14}H_9D$), *d*-phenanthrene ($C_{14}H_9D$), *d*-pyrene ($C_{16}H_9D$), *d*-perylene ($C_{20}H_{11}D$), and *d*-coronene ($C_{24}H_{11}D$). For each PAH species,

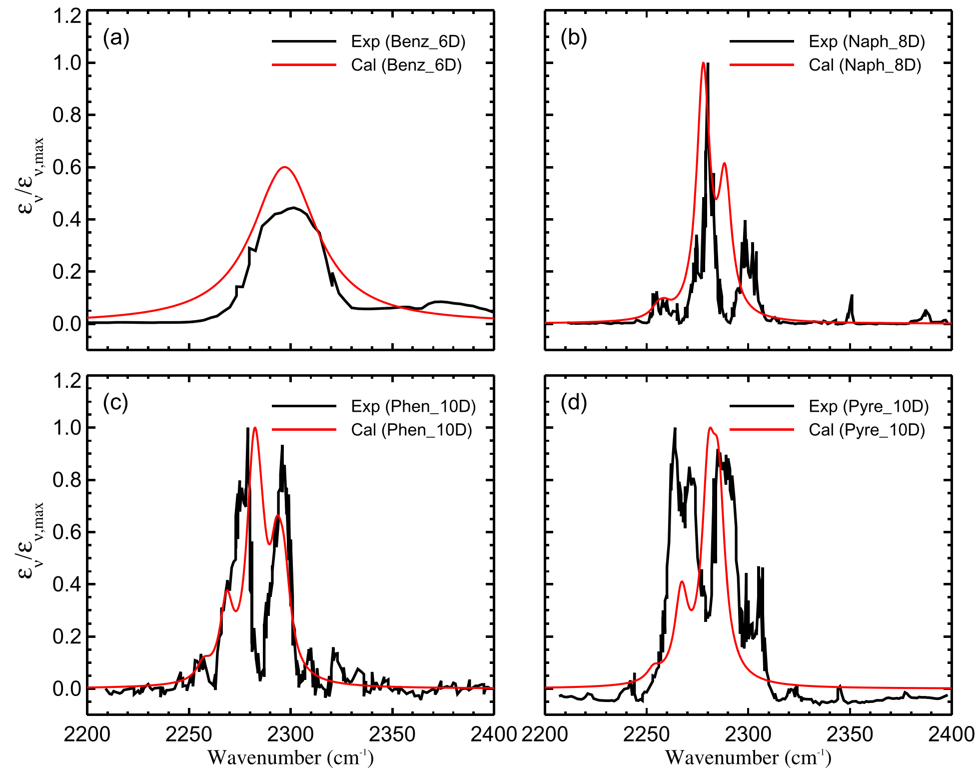

Figure 4. Comparison of the experimental spectra in the C–D stretching region (black solid lines) of perdeuterated benzene (a), naphthalene (b), phenanthrene (c), and pyrene (d) with those computed from B3LYP/6-311+G** (red solid lines). Panel (a) is a zoomed-in view of the C–D stretch of perdeuterated benzene shown in Figure 3. While the experimental spectrum of perdeuterated benzene is taken from the NIST webbook, the experimental spectra of the other three perdeuterated species are taken from Bauschlicher et al. (1997). The calculated frequencies are scaled with a factor of 0.9688 and a line width of 4 cm^{-1} is assigned for perdeuterated naphthalene, phenanthrene, and pyrene, while a scale factor of 0.9748 and a line width of 20 cm^{-1} are applied to benzene. To facilitate comparison, we normalize the experimental and computational spectra to their maxima since the experimental spectra do not have information for the (absolute) intensities.

Table 1
Comparison of the Experimental and Computational Frequencies and Relative Intensities of the C–D Bands for Perdeuterated PAHs

Vibrational Mode	Molecule	Experimental		Calculational		
		$\tilde{\nu}$ (cm^{-1})	$A_{CD}/A_{CD,oop}$	$\tilde{\nu}$ (cm^{-1})	A_{CD} (km mol^{-1})	$A_{CD}/A_{CD,oop}$
C–D oop bending	Naph_8D	630.9, 634.3	1.00	620.6	6.16	1.00
	Phen_10D	610.7	1.00	601.8, 638.5	4.23	1.00
	Pyre_10D	604.0	1.00	593.1	5.09	1.00
C–D in-plane bending	Naph_8D	829.8, 832.5	0.17	816.6, 824.3	0.97	0.16
	Phen_10D	834.5	0.44	821.1, 830.9	0.91	0.21
	Pyre_10D	841.3	0.18	822.3, 828.3	0.96	0.19
C–D stretching	Naph_8D	2250 ~ 2315	1.12	2255 ~ 2288	6.91	1.12
	Phen_10D	2249 ~ 2311	1.42	2253 ~ 2297	6.61	1.56
	Pyre_10D	2245 ~ 2313	1.51	2253 ~ 2285	7.64	1.50

we consider all the monodeuterated isomers of which each has a different position of D atom attachment (see Figure 1). The calculated spectra are shown in Figures 5–11. The frequencies are scaled with a factor of 0.9688, and the line widths are taken to be 10 cm^{-1}.[8] To highlight the C–D features, we also show in the corresponding panels the IR spectra computed for pure PAHs.

As expected, the C–D stretching features are apparent in the computed spectra at ~4.4 μm (i.e., 2270 cm^{-1}) of all the deuterated derivatives. The frequencies of the C–D stretch for the deuterated cations are somewhat blueshifted with respect to the neutrals, with an average wavelength of ~4.40 μm for the neutrals and ~4.37 μm for the cations. The C–H stretch also shows a similar behavior for both pure and deuterated PAHs, with an average wavelength of ~3.25 μm for the neutrals and ~3.22 μm for the cations. Meanwhile, the C–D and C–H stretches of the cations are significantly suppressed with respect to the neutrals, just like pure PAHs (e.g., see Allamandola et al. 1999),

[8] Such a line width of 10 cm^{-1} is adopted to distinctly reveal the major C–H, C–D, and C–C vibrational bands in the computational spectra. Too large a line width would lead to the clumping of some of the major bands and hence difficulty in identifying individual bands. We note that we assign a line width of 20 cm^{-1} for Benz_6D (see Section 3.1, Figures 3(a) and 4(a)) and 4 cm^{-1} for Naph_8D, Phen_10D and Pyre_10D (see Section 3.1, and Figure 4(a)) since the computational spectra with these line widths best match the experimental spectra.

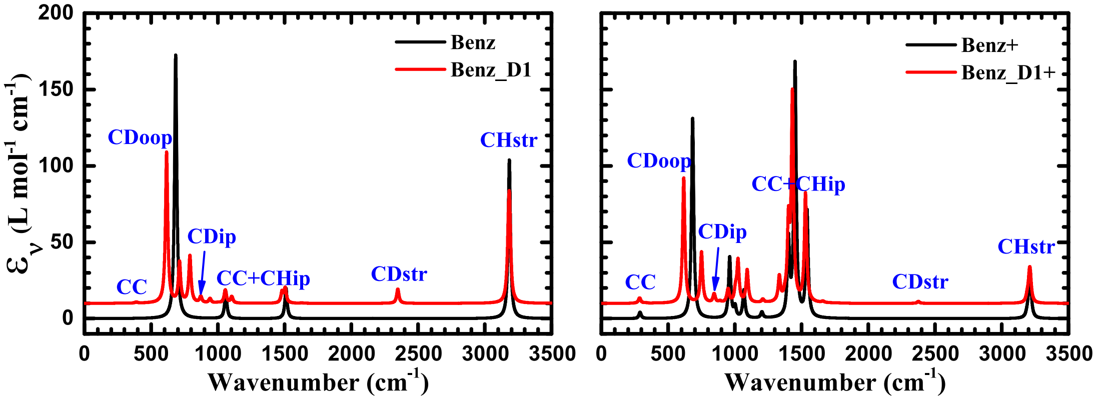

Figure 5. Comparison of the computational spectra (red lines) of monodeuterated benzene (left panel) and its cation (right panel) with that of pure benzene and its cation (black lines). The frequencies are scaled with a factor of 0.9688, and a line width of 10 cm^{-1} is assigned. The computational spectra are expressed in terms of molar extinction coefficient $\varepsilon_{\tilde{\nu}}$ which relates to the absorption cross sections $C_{abs}(\lambda)$ through Equation (1). The major vibrational bands are labeled as CDstr, CDip, CDoop, CHstr, and CHip (C–H in-plane bending bands).

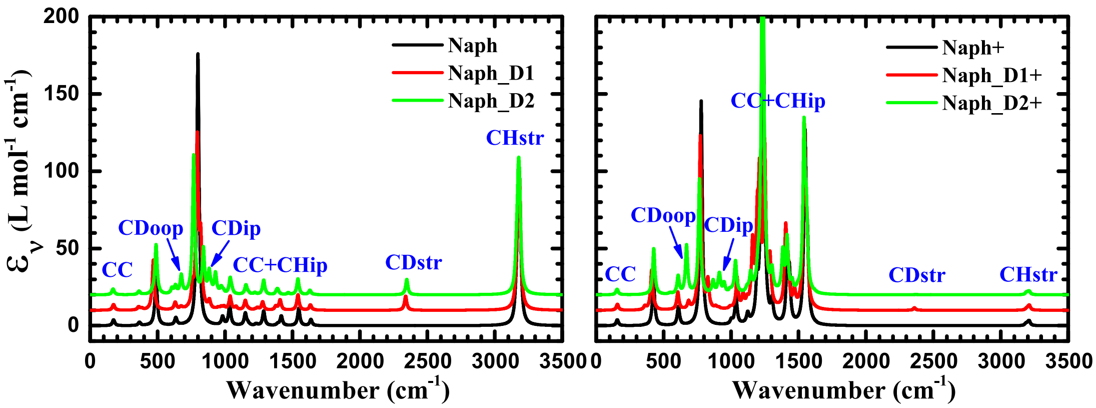

Figure 6. Comparison of the computational spectra (red and green lines) of monodeuterated naphthalene (left panel) and its cation (right panel) with that of pure naphthalene and its cation (black lines). The frequencies are scaled with a factor of 0.9688, and a line width of 10 cm^{-1} is assigned.

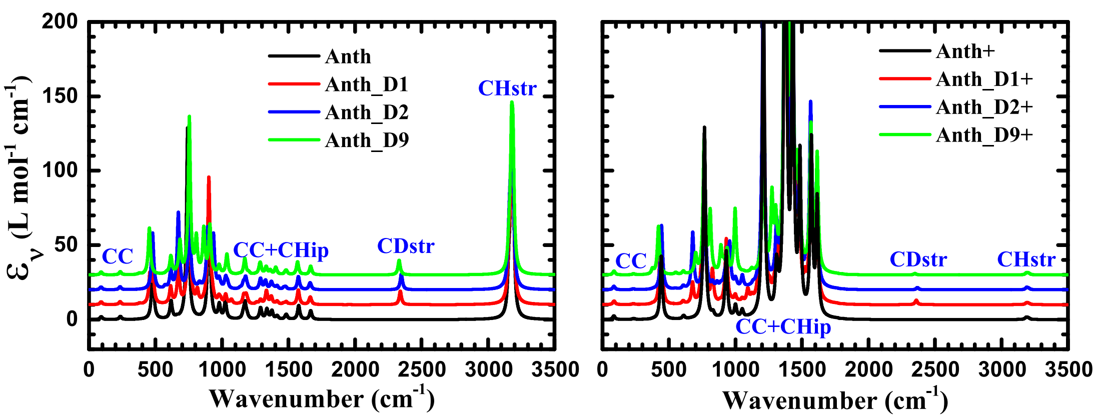

Figure 7. Comparison of the computational spectra (red, blue, and green lines) of monodeuterated anthracene (left panel) and its cation (right panel) with that of pure anthracene and its cation (black lines). The frequencies are scaled with a factor of 0.9688, and a line width of 10 cm^{-1} is assigned.

superhydrogenated PAHs (Yang et al. 2020), and PAHs with aliphatic functional groups (Yang et al. 2017). Let $A_{3.3}$ and $A_{4.4}$ respectively be the intrinsic band strengths of the aromatic C–H and C–D stretches on a per bond basis. For the neutrals, the average $A_{3.3}$ and $A_{4.4}$ are respectively $\sim$13.22 km mol^{-1} and $\sim$7.29 km mol^{-1}, and $\sim$0.63 km mol^{-1} and $\sim$1.38 km mol^{-1} for the cations.

The C–D oop bending ($\sim$15.4 μm) and in-plane bending ($\sim$11.7 μm) features are well mixed with the C–C–C or C–H related features, e.g., the latter often overlaps with the C–H oop bending features (see Hudgins et al. 2004). Therefore, it is difficult to identify the C–D in-plane and oop bending bands from the computed IR spectra since these features lie so close to the C–H and C–C–C bands that no matter how small a line width is assigned, these features always overlap. Nevertheless, we can still identify them from the Gaussian09 output files and read their frequencies and intensities, as tabulated in Tables 2 and 3. For both neutrals and cations, the frequencies

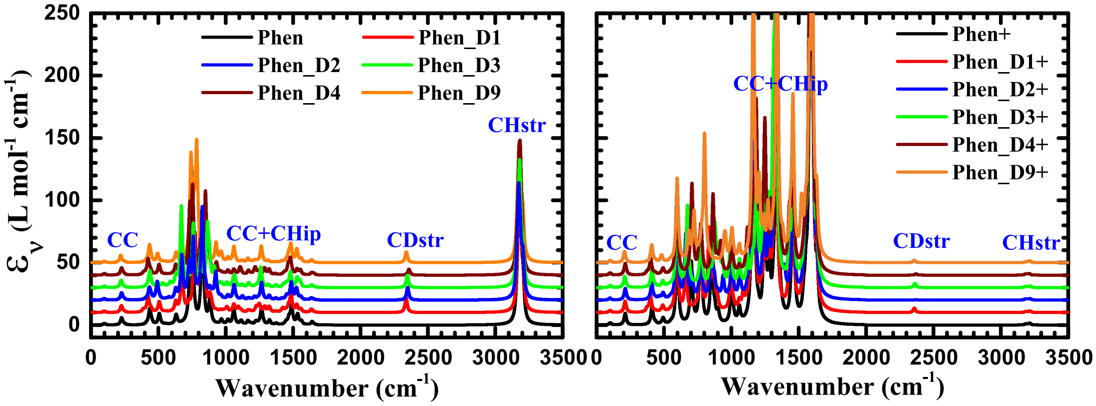

Figure 8. Comparison of the computational spectra (red, blue, brown, green, and yellow lines) of monodeuterated phenanthrene (left panel) and its cation (right panel) with that of pure phenanthrene and its cation (black lines). The frequencies are scaled with a factor of 0.9688, and a line width of 10 cm^{-1} is assigned.

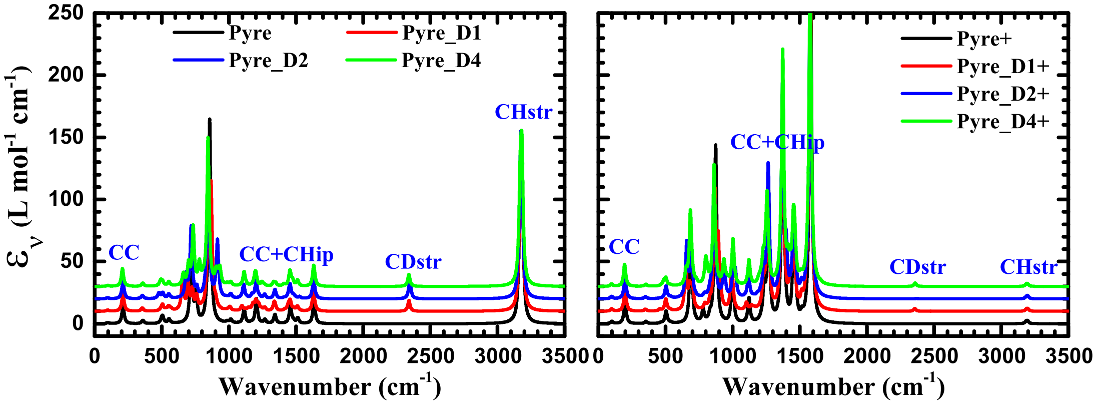

Figure 9. Comparison of the computational spectra (red, blue, and green lines) of monodeuterated pyrene (left panel) and its cation (right panel) with that of pure pyrene and its cation (black lines). The frequencies are scaled with a factor of 0.9688, and a line width of 10 cm^{-1} is assigned.

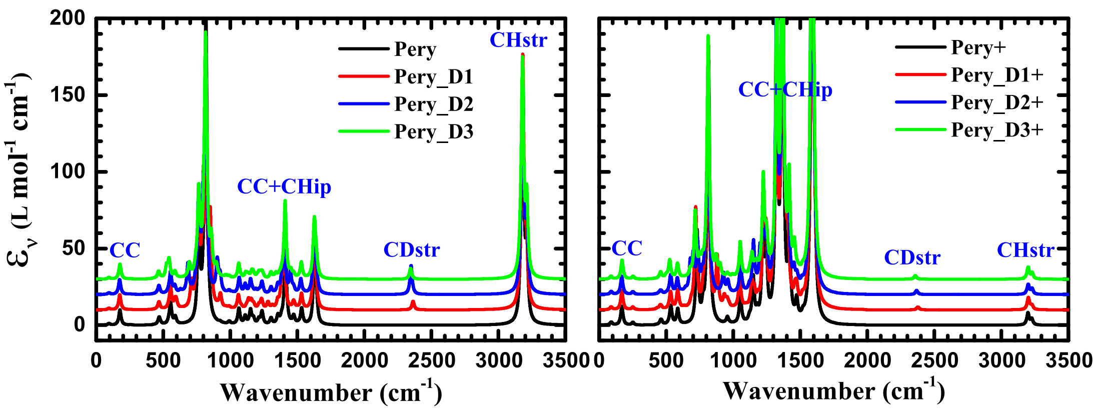

Figure 10. Comparison of the computational spectra (red, blue, and green lines) of monodeuterated perylene (left panel) and its cation (right panel) with that of pure perylene and its cation (black lines). The frequencies are scaled with a factor of 0.9688, and a line width of 10 cm^{-1} is assigned.

are basically in the wavenumber range of ∼830–960 cm^{-1} for the C–D in-plane bending modes and ∼600–675 cm^{-1} for the C–D oop bending modes.

For both neutrals and cations, the band strengths of these two vibrational modes scatter significantly from one molecule to another, with the standard deviations at the same order of magnitude as the average values (see Tables 2 and 3). Moreover, the vibrations of the C–D oop bending and in-plane bending are usually coupled with other vibrational modes. For these reasons, we will not discuss the intensities of the C–D bending modes any further.

4. Astrophysics Implications

4.1. Aromatic C–H and C–D Band Intensities of Deuterated PAHs

We show in Figure 12 the intensities of the aromatic C–H and C–D stretches computed for 18 monodeuterated *neutral* PAH species. These species are displayed in the order of their (increasing) sizes from benzene, naphthalene, etc., up to coronene. For the same parental molecule, the isomers are displayed in the order of the position where the D atom is attached (e.g., from Phen_D1, Phen_D2, etc., to Phen_D9). Except for one species

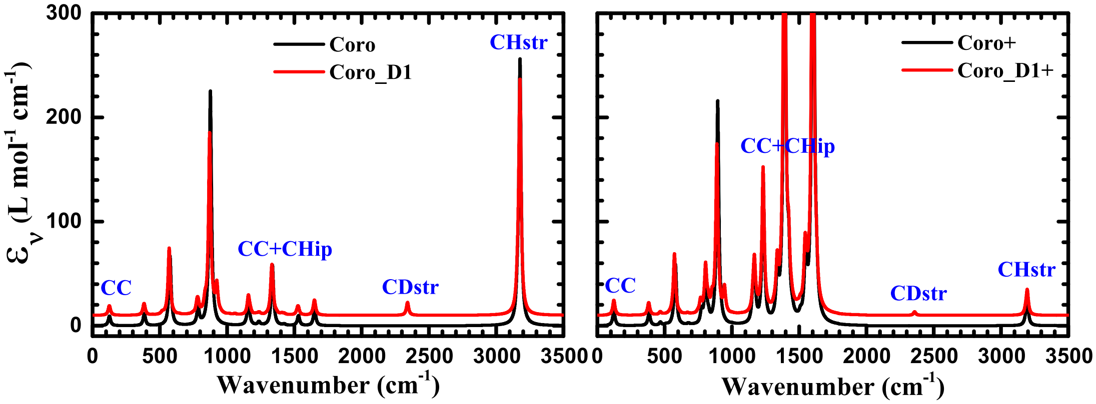

Figure 11. Comparison of the computational spectra (red lines) of monodeuterated coronene (left panel) and its cation (right panel) with that of pure coronene and its cation (black lines). The frequencies are scaled with a factor of 0.9688, and a line width of 10 cm^{-1} is assigned.

Table 2
Wavelengths (λ) and Intensities (A_λ) of the Nominal 3.3 μm C–H Stretching, 4.4 μm C–D Stretching, 11.7 μm C–D In-plane Bending, and 15.4 μm C–D OOP Bending Bands Computed at the B3LYP/6-311+G** Level for All the Neutral Monodeuterated PAHs Shown in Figure 1

Compound	$\lambda_{3.3}$ (μm)	$A_{3.3}$ (km mol^{-1})	$\lambda_{4.4}$ (μm)	$A_{4.4}$ (km mol^{-1})	$A_{4.4}/A_{3.3}$	$\lambda_{11.7}$ (μm)	$A_{11.7}$ (km mol^{-1})	$\lambda_{15.4}$ (μm)	$A_{15.4}$ (km mol^{-1})
Benz_D1	3.24	12.55	4.40	6.78	0.54	11.84	2.91	16.76	71.34
Naph_D1	3.25	12.98	4.41	6.62	0.51	11.67	2.77	15.31	1.15
Naph_D2	3.25	12.71	4.40	7.13	0.56	11.48	1.68	15.28	8.50
Anth_D1	3.25	13.37	4.41	6.53	0.49	11.70	2.03	15.35	18.72
Anth_D2	3.25	12.96	4.39	7.73	0.60	11.66	2.07	15.37	36.57
Anth_D9	3.25	13.45	4.43	7.11	0.53	10.52	0.41	15.10	15.40
Phen_D1	3.24	12.25	4.41	8.51	0.69	11.55	2.97	15.29	25.58
Phen_D2	3.24	12.19	4.39	7.31	0.60	11.46	1.78	15.32	24.78
Phen_D3	3.24	12.29	4.40	7.25	0.59	11.33	2.76	15.39	46.35
Phen_D4	3.24	13.08	4.37	3.40	0.26	11.09	6.24	15.19	10.11
Phen_D9	3.24	12.52	4.41	6.28	0.50	10.72	2.63	15.41	0.21
Pyre_D1	3.25	14.21	4.41	6.30	0.44	11.45	3.48	15.76	19.46
Pyre_D2	3.25	13.37	4.40	11.48	0.86	11.54	0.53	15.17	12.85
Pyre_D4	3.25	14.10	4.41	6.97	0.49	11.12	2.16	15.62	6.53
Pery_D1	3.24	13.78	4.37	4.05	0.29	11.13	5.61	…	…
Pery_D2	3.24	12.50	4.39	13.72	1.10	11.44	0.79	15.09	13.46
Pery_D3	3.24	13.47	4.40	5.11	0.38	11.52	4.72	14.88	6.31
Coro_D1	3.25	16.20	4.41	8.96	0.55	11.45	2.13	…	…
Average	3.25	13.22	4.40	7.29	0.56	11.37	2.65	15.39	19.83
Stdev	0.00	0.97	0.01	2.39	0.19	0.34	1.59	0.42	18.48

Note. The intensities, A_λ, relate to the molar extinction coefficients $\varepsilon_{\tilde{\nu}}$ through Equation (2).

(i.e., Coro_D1), the band strength of the C–H stretch at 3.3 μm on a per unit C–H bond basis does not vary much among different molecules. On average, these monodeuterated neutral PAH species (including Coro_D1) have a mean (per bond) band strength of $\langle A_{3.3}\rangle \approx 13.2 \pm 1.0$ km mol^{-1}. The band strength of the C–D stretch at 4.4 μm, on a per unit C–D bond basis, $A_{4.4}$, exhibits more appreciable variations than $A_{3.3}$ among these 18 species, with three species (i.e., Phen_D4, Pyre_D2 and Pery_D2) noticeably deviating from the majority. On average, these monodeuterated neutral species have a mean band strength of $\langle A_{4.4}\rangle \approx 7.3 \pm 2.4$ km mol^{-1}. For these monodeuterated neutral PAHs, the mean band-strength ratio of the C–D stretch to the C–H stretch is $\langle A_{4.4}/A_{3.3}\rangle \approx 0.56 \pm 0.19$.

Similarly, we show in Figure 13 the band strengths of the C–H and C–D stretches computed for 18 monodeuterated *cationic* PAH species. Except for one species (i.e., Benz_D1), $A_{3.3}$ varies very little among different molecules. In contrast, $A_{4.4}$ exhibits more significant variations. With $\langle A_{3.3}\rangle \approx 0.63^{+1.01}_{-0.63}$ km mol^{-1} and $\langle A_{4.4}\rangle \approx 1.38 \pm 0.77$ km mol^{-1}, it is apparent that cationic PAHs have their C–H and C–D stretches substantially suppressed compared to their neutral counterparts. For these monodeuterated cationic PAHs the mean C–D to C–H band-strength ratio is, on average, $\langle A_{4.4}/A_{3.3}\rangle \approx 4.9 \pm 4.5$.

For monodeuterated neutral PAHs, at first glance, it appears that large, compact, pericondensed PAHs intend to exhibit more appreciable variations in the C–D stretching band strength $A_{4.4}$ (see Figure 12). However, a close inspection of Figure 13 reveals that, for monodeuterated PAH cations, small, catacondensed PAHs also exhibit appreciable variations in $A_{4.4}$. Apparently, a simple dependence of $A_{4.4}$ on the PAH size and structure does not seem to exist.

In Table 4 we summarize the *mean* band strengths of the C–H and C–D stretches computed for monodeuterated PAHs, obtained by averaging over all the monodeuterated species,

Table 3
Same as Table 2 but for Monodeuterated Cationic PAHs

Compound	$\lambda_{3.3}$ (μm)	$A_{3.3}$ (km mol^{-1})	$\lambda_{4.4}$ (μm)	$A_{4.4}$ (km mol^{-1})	$A_{4.4}/A_{3.3}$	$\lambda_{11.7}$ (μm)	$A_{11.7}$ (km mol^{-1})	$\lambda_{15.4}$ (μm)	$A_{15.4}$ (km mol^{-1})
Benz_D1+	3.22	4.37	4.35	0.89	0.20	12.22	4.11	16.73	59.30
Naph_D1+	3.22	0.48	4.37	1.14	2.36	11.64	1.00	15.06	3.31
Naph_D2+	3.22	0.42	4.35	0.20	0.47	11.42	1.18	15.40	22.61
Anth_D1+	3.23	0.17	4.37	2.14	12.69	11.65	0.00	15.25	10.03
Anth_D2+	3.23	0.20	4.36	1.10	5.65	12.02	1.12	15.74	27.35
Anth_D9+	3.23	0.20	4.39	0.69	3.47	10.35	27.75	14.73	9.01
Phen_D1+	3.22	0.18	4.38	2.54	14.06	11.50	1.63	15.61	27.58
Phen_D2+	3.22	0.20	4.35	0.26	1.32	11.43	2.07	15.58	36.72
Phen_D3+	3.22	0.19	4.37	2.42	12.53	11.30	11.24	15.32	46.46
Phen_D4+	3.23	0.18	4.35	0.72	4.11	11.21	16.84	15.05	0.12
Phen_D9+	3.22	0.19	4.38	1.47	7.86	10.80	12.15	15.08	15.93
Pyre_D1+	3.23	0.24	4.38	1.59	6.59	11.38	7.12	15.87	24.25
Pyre_D2+	3.23	0.26	4.35	0.21	0.81	11.47	0.32	15.69	31.48
Pyre_D4+	3.23	0.23	4.38	1.93	8.39	11.10	3.11	15.80	7.32
Pery_D1+	3.22	0.72	4.34	1.40	1.95	11.06	4.54	17.45	2.12
Pery_D2+	3.22	0.68	4.36	1.96	2.88	11.35	0.57	15.19	12.75
Pery_D3+	3.22	0.77	4.38	1.74	2.26	11.45	5.11	15.20	2.92
Coro_D1+	3.23	1.76	4.38	2.40	1.36	11.33	0.16	14.81	0.15
Average	3.22	0.63	4.37	1.38	4.94	11.37	5.56	15.53	18.86
Stdev	0.01	1.01	0.01	0.77	4.47	0.41	7.30	0.67	16.97

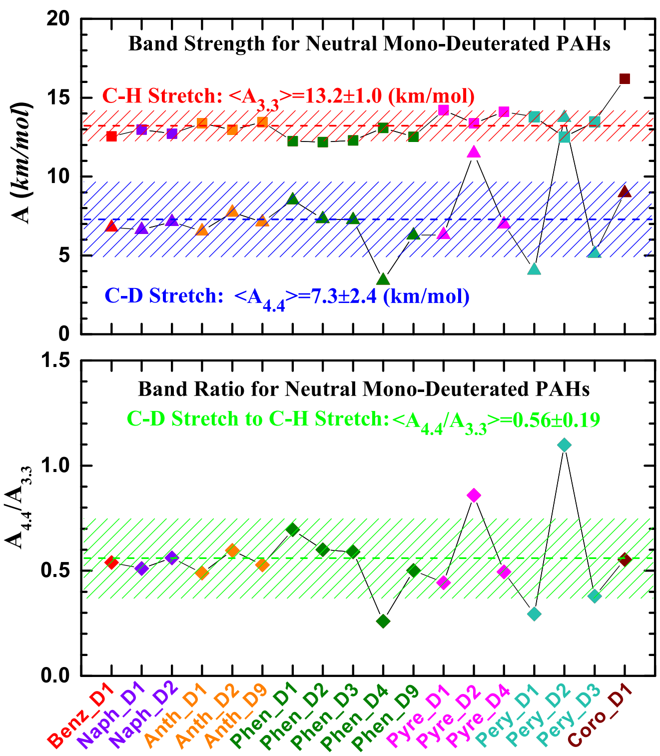

Figure 12. Band strengths of the 3.3 μm C–H stretches ($A_{3.3}$) and the 4.4 μm C–D stretches ($A_{4.4}$) as well as the band-strength ratios $A_{4.4}/A_{3.3}$ computed at level B3LYP/6-311+G** for the monodeuterated *neutral* PAH molecules shown in Figure 1.

with recommended values of $\langle A_{3.3}\rangle \approx 13.2 \pm 1.0$ km mol^{-1}, $\langle A_{4.4}\rangle \approx 7.3 \pm 2.4$ km mol^{-1}, and $\langle A_{4.4}/A_{3.3}\rangle \approx 0.56 \pm 0.19$ for neutral PAHs, and $\langle A_{3.3}\rangle \approx 0.63^{+1.01}_{-0.63}$ km mol^{-1}, $\langle A_{4.4}\rangle \approx 1.38 \pm 0.77$ km mol^{-1}, and $\langle A_{4.4}/A_{3.3}\rangle \approx 4.94 \pm 4.47$ for cations.

4.2. Deuterium Depletion onto PAHs

Let $[\mathrm{D/H}]_{\mathrm{PAH}}$ be the degree of deuteration of PAHs. For a deuterated PAH molecule containing N_{C} aromatic C atoms, N_{H} H atoms, and N_{D} D atoms, we define the degree of deuteration of the molecule as $[\mathrm{D/H}]_{\mathrm{PAH}} \equiv N_{\mathrm{D}}/(N_{\mathrm{H}} + N_{\mathrm{D}})$. Letting $(I_{4.4}/I_{3.3})_{\mathrm{obs}}$ be the *observed* ratio of the power emitted from the 4.4 μm aromatic C–D feature ($I_{4.4}$) to that from the 3.3 μm aromatic C–H feature ($I_{3.3}$), we have

$$\left(\frac{I_{4.4}}{I_{3.3}}\right)_{\mathrm{obs}} \approx \left(\frac{A_{4.4}}{A_{3.3}}\right) \times \left(\frac{N_{\mathrm{C-D}}}{N_{\mathrm{C-H}}}\right) \times \left(\frac{B_{4.4}}{B_{3.3}}\right), \tag{3}$$

where $N_{\mathrm{C-H}}$ and $N_{\mathrm{C-D}}$ are respectively the number of C–H and C–D bonds in a deuterated PAH molecule, $B_{\lambda}(T)$ is the Planck function at wavelength λ and temperature T, and $A_{3.3}$ and $A_{4.4}$ are the intrinsic band strengths of the aromatic C–H and C–D stretches (on a per C–H or C–D bond basis). Since, as discussed earlier (see Sections 3.2 and 4.1), the C–H and C–D stretching features are predominantly emitted by neutral PAHs, we will adopt $A_{4.4}/A_{3.3} \approx 0.56 \pm 0.19$ (see Section 4.1 and Table 4).

Assuming in a PAH molecule all the D and H atoms are attached to aromatic C atoms, then $N_{\mathrm{C-D}} = N_{\mathrm{D}}$ and $N_{\mathrm{C-H}} = N_{\mathrm{H}}$,[9] the degree of deuteration of the molecule

[9] We note that interstellar PAHs could be superhydrogenated (Bernstein et al. 1996; Sandford et al. 2013; Yang et al. 2020) or attached with aliphatic functional groups (Geballe et al. 1985; Sandford 1991; Sandford et al. 1991; Kwok & Zhang 2011; Yang et al. 2017), which could convert the aromatic C atoms to aliphatic. However, we have shown that the degree of superhydrogenation (Yang et al. 2020) and the aliphatic content of PAHs are minor (Li & Draine 2012; Yang et al. 2013, 2017). Nevertheless, the aliphatic C–D stretches at 4.65 and 4.75 μm appear to be present in the ISO/SWS and AKARI/IRC spectra of several interstellar objects (Peeters et al. 2004; Onaka et al. 2014; Doney et al. 2016), indicating that some D atoms may be attached to aliphatic C atoms.

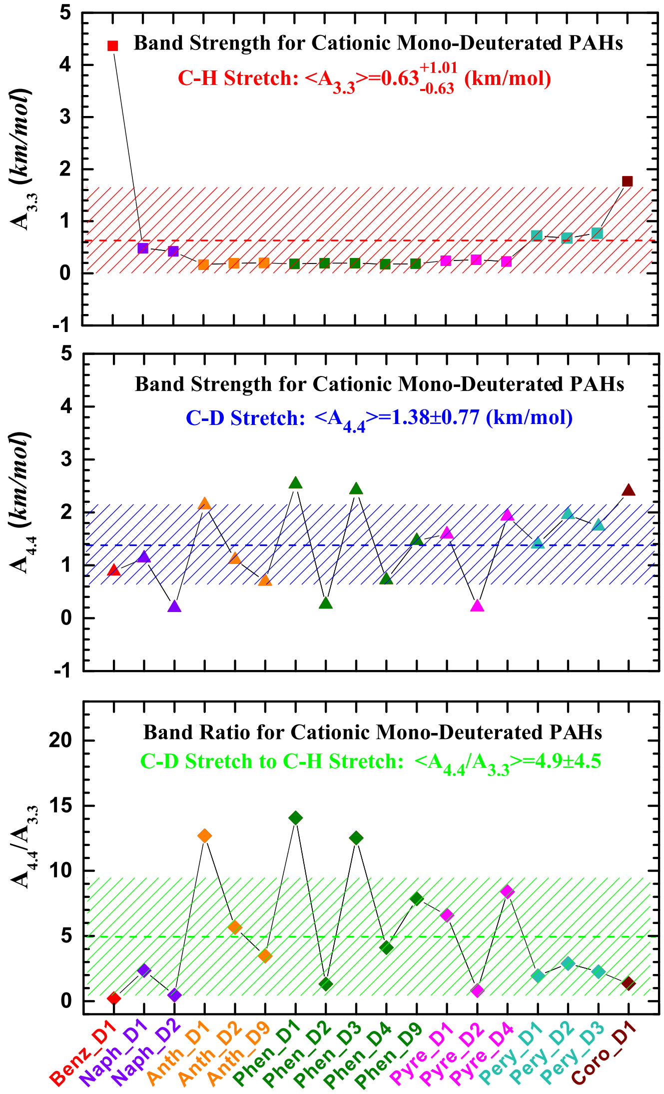

Figure 13. Band strengths of the 3.3 μm C–H stretches ($A_{3.3}$) and the 4.4 μm C–D stretches ($A_{4.4}$) as well as the band-strength ratios $A_{4.4}/A_{3.3}$ computed at level B3LYP/6-311+G** for the cationic counterparts of the monodeuterated PAHs shown in Figure 1.

Table 4
Mean Intensities of the 3.3 μm Aromatic C–H Stretch ($A_{3.3}$) and the 4.4 μm Aromatic C–D Stretch ($A_{4.4}$) Computed at the B3LYP/6-311+G** Level for All the Monodeuterated PAHs Shown in Figure 1

Band Strengths	Neutral PAHs	Cationic PAHs
$A_{3.3}$ (km mol^{-1})	13.2 ± 1.0	$0.63^{+1.01}_{-0.63}$
$A_{4.4}$ (km mol^{-1})	7.3 ± 2.4	1.38 ± 0.77
$A_{4.4}/A_{3.3}$	0.56 ± 0.19	4.94 ± 4.47

Note. The $A_{3.3}$ and $A_{4.4}$ band strengths are on a per C–H or C–D bond basis.

becomes

$$[\mathrm{D/H}]_{\mathrm{PAH}} \approx \left\{1 + \left(\frac{I_{3.3}}{I_{4.4}}\right)_{\mathrm{obs}} \times \left(\frac{A_{4.4}}{A_{3.3}}\right) \times \left(\frac{B_{4.4}}{B_{3.3}}\right)\right\}^{-1}. \quad (4)$$

The 3.3 μm C–H stretch and 4.4 μm C–D stretch are most effectively emitted by PAHs of vibrational temperatures of $\sim$728 K and $\sim$546 K, respectively, stochastically heated by individual ultraviolet photons (Draine & Li 2001).[10] For $546 \lesssim T \lesssim 728$ K, we obtain $B_{3.3}/B_{4.4} \approx 0.75 \pm 0.10$. By relaxing the temperature range to $400 \lesssim T \lesssim 900$ K, we obtain $B_{3.3}/B_{4.4} \approx 0.70 \pm 0.28$.[11] In the following, we will adopt $B_{3.3}/B_{4.4} \approx 0.70 \pm 0.28$ (suitable for $400 \lesssim T \lesssim 900$ K).

Many observational efforts have been made to detect deuterated PAHs through their vibrational C–D bands. Peeters et al. (2004) searched for the C–D emission feature of deuterated PAHs in the Orion Bar and M17 photodissociation regions (PDRs). Based on ISO/SWS observations, Peeters et al. (2004) reported detection of weak emission features at 4.4 and 4.65 μm in the Orion Bar. In M17, they confirmed the earlier detection of the weak emission feature at 4.65 μm reported by Verstraete et al. (1996). Peeters et al. (2004) attributed the 4.4 μm feature to the aromatic C–D stretch in deuterated PAHs and the 4.65 μm feature to the aliphatic C–D stretch in superdeuterated PAHs or PAHs with deuterated aliphatic side groups. Onaka et al. (2014) have also searched for the C–D emission feature of deuterated PAHs in the Orion Bar and M17 as well as in G18.14.0, a reflection nebula, based on the near-IR spectroscopy at $\sim$2.5–5 μm obtained by AKARI/IRC. Also with AKARI/IRC, Doney et al. (2016) have performed a deuterated PAH survey in 53 H II regions in the Milky Way, Large Magellanic Cloud and Small Magellanic Cloud. They reported the detection of deuterated PAHs in six sources, as revealed by the asymmetric aliphatic C–D stretch at $\sim$4.63 μm and the symmetric aliphatic C–D stretch at $\sim$4.75 μm, in addition to the aromatic C–D stretching emission band at 4.4 μm.

We have compiled all the available observational data on $(I_{4.4}/I_{3.3})_{\mathrm{obs}}$ (Peeters et al. 2004; Onaka et al. 2014; Doney et al. 2016) and summarized these data in Table 5. On average, we obtain $\langle (I_{4.4}/I_{3.3})_{\mathrm{obs}} \rangle \approx 0.019$. With $B_{3.3}/B_{4.4} \approx 0.70 \pm 0.28$, we obtain from $(I_{4.4}/I_{3.3})_{\mathrm{obs}} \approx 0.019$ a deuteration degree of $[\mathrm{D/H}]_{\mathrm{PAH}} \approx 2.4\%$ for neutral PAHs of $A_{4.4}/A_{3.3} \approx 0.56 \pm 0.16$. Compared to the interstellar abundance of $[\mathrm{D/H}]_{\mathrm{ISM}} \approx 2 \times 10^{-5}$, this implies a D enrichment in PAHs by a factor of $[\mathrm{D/H}]_{\mathrm{PAH}}/[\mathrm{D/H}]_{\mathrm{ISM}} \approx 1200$.

We note that the actual degree of deuteration in PAHs could be higher than 2.4% since some D atoms may be incorporated into PAHs to generate aliphatic C–D bands, either in the form of excess D atoms attached to fully hydrogenated or superhydrogenated PAHs (Hudgins et al. 2004; Buragohain et al. 2015, 2016) or in the form of D-substituted aliphatic side groups (Buragohain et al. 2020). Both experimental measurements and DFT-based computations have demonstrated that the IR spectra of such D-containing PAHs exhibit a prominent aliphatic C–D stretching band at $\sim$4.6–4.8 μm (Hudgins et al. 2004; Buragohain et al. 2015, 2016, 2020). Indeed, ISO/SWS and AKARI/IRC observations have shown that whenever the 4.4 μm aromatic C–D band was detected, an accompanying aliphatic C–D band was also detected. The latter is often stronger than the former by a factor of $\sim$2–7 (Peeters et al. 2004; Doney et al. 2016). This suggests that a

[10] Let $C_{\mathrm{abs}}(\lambda)$ be the dust absorption cross section at wavelength λ and j_λ be the dust IR emissivity. For $C_{\mathrm{abs}}(\lambda) \propto \lambda^{-\beta}$, λj_λ peaks at $\lambda_p \approx (hc/kT)/(4+\beta)$, where h is the Planck constant, c is the speed of light, and k is the Boltzmann constant (see Li 2009). With $\beta \approx 2$ for PAH-like molecules, we have $T \approx 728$ K for $\lambda_p \sim 3.3$ μm and $T \approx 546$ K for $\lambda_p \sim 4.4$ μm.

[11] Even if we extend the temperature range to $300 \lesssim T \lesssim 1000$ K, $B_{3.3}/B_{4.4} \approx 0.63 \pm 0.38$ is only lower by $\sim$10%.

Table 5
A Summary of the Power Emitted from the 3.3 μm Aromatic C–H Band $(I_{3.3})_{\rm obs}$ and the 4.4 μm Aromatic C–D Band $(I_{4.4})_{\rm obs}$ Compiled from All the Observational Data Available in the Literature

Object	Type	$(I_{3.3})_{\rm obs}$ (10^{-17} W m^{-2} arcsec^{-2})	$(I_{4.4})_{\rm obs}$ (10^{-17} W m^{-2} arcsec^{-2})	$(I_{4.4}/I_{3.3})_{\rm obs}$
G75.78 + 0.34[a]	H II Region	22.20 ± 2.00	0.30 ± 0.19	1.35% ± 0.73%
NGC 3603[a]	H II Region	25.10 ± 2.40	0.62 ± 0.52	2.47% ± 1.84%
W51 obs. 1[a]	H II Region	20.00 ± 1.80	0.41 ± 0.14	2.05% ± 0.52%
W51 obs. 2[a]	H II Region	20.60 ± 1.80	0.16 ± 0.14	0.78% ± 0.61%
M8[a]	H II Region	99.10 ± 8.90	1.03 ± 0.53	1.04% ± 0.44%
IRAS 112073 obs. 1[a]	H II Region	11.70 ± 1.00	0.30 ± 0.08	2.56% ± 0.46%
IRAS 112073 obs. 2[a]	H II Region	12.20 ± 1.00	0.37 ± 0.08	3.03% ± 0.41%
Orion Bar[b]	PDR	53.10 ± 0.60	1.36 ± 0.11	2.56% ± 0.18%
M17[b]	PDR	14.90 ± 0.20	1.40 ± 0.04	0.94% ± 0.26%
G18.14.0[b]	Reflection Nebula	4.78 ± 0.06	0.12 ± 0.01	2.45% ± 0.20%

Notes.
[a] Doney et al. (2016).
[b] Onaka et al. (2014).

significant number of D atoms may be attached to aliphatic C atoms.[12] Also, the current estimation is based on the 3.3 and 4.4 μm features, which are only sensitive to small PAHs. If an appreciable number of D atoms reside in large PAHs, they will emit mainly at longer wavelengths through C–D oop and in-plane bending modes. Future observational studies with JWST of both aliphatic and aromatic C–D stretching bands and aromatic C–D oop and in-plane bending bands will be highly valuable.

5. Summary

To facilitate a quantitative understanding of PAHs as a possible reservoir of interstellar D, we have employed the hybrid DFT method B3LYP in conjunction with the 6-311+G** basis set to calculate the IR vibrational spectra of singly deuterated PAHs and their cations of various sizes (from benzene and naphthalene to perylene and coronene). The major results are as follows:

1. The aromatic C–D stretching, in-plane bending and oop bending bands are seen at ∼4.4 μm, ∼11.7 μm, and ∼15.4 μm, respectively, in all the deuterated PAH species.
2. For all these monodeuterated species, we have derived from the computed spectra the intrinsic band strengths of the 3.3 μm aromatic C–H stretch ($A_{3.3}$) and the 4.4 μm aromatic C–D stretch ($A_{4.4}$). Both the C–H and C–D stretches predominantly arise from neutral PAHs. By averaging over all these molecules, we have determined the mean band strengths to be $\langle A_{3.3}\rangle \approx 13.2 \pm 1.0$ km mol^{-1} and $\langle A_{4.4}\rangle \approx 7.3 \pm 2.4$ km mol^{-1} for neutral PAHs, and $\langle A_{3.3}\rangle \approx 0.63^{+1.01}_{-0.63}$ km mol^{-1} and $\langle A_{4.4}\rangle \approx 1.38 \pm 0.77$ km mol^{-1} for cationic PAHs. The mean band-strength ratios of the C–D stretch to the C–H stretch are $\langle A_{4.4}/A_{3.3}\rangle \approx 0.56 \pm 0.19$ for the neutrals, and $\langle A_{4.4}/A_{3.3}\rangle \approx 4.94 \pm 4.47$ for the cations.
3. We have also derived from the monodeuterated species the intrinsic strengths of the 11.7 μm aromatic C–D in-plane bending band ($A_{11.7}$) and the 15.4 μm aromatic C–D oop bending band ($A_{15.4}$). By averaging over all these monodeuterated species, we have determined the mean band strengths to be $\langle A_{11.7}\rangle \approx 2.65$ km mol^{-1} and $\langle A_{15.4}\rangle \approx 19.8$ km mol^{-1} for the neutrals, and $\langle A_{11.7}\rangle \approx 5.56$ km mol^{-1} and $\langle A_{15.4}\rangle \approx 18.86$ km mol^{-1} for the cations.
4. We have compiled all the observational data from ISO/SWS and AKARI/IRC and derived the ratio of the power emitted from the astronomical 4.4 μm aromatic C–D feature ($I_{4.4}$) to that from the astronomical 3.3 μm aromatic C–H feature ($I_{3.3}$) to be $\langle (I_{4.4}/I_{3.3})_{\rm obs}\rangle \approx 0.019$. By comparing the computationally derived mean ratio of $\langle A_{4.4}/A_{3.3}\rangle \approx 0.56$ for neutral deuterated PAHs, we have estimated the degree of deuteration to be $[{\rm D/H}]_{\rm PAH} \approx 2.4\%$ for neutral PAHs which dominate the emission at the C–H and C–D stretching bands. Compared to the interstellar abundance of $[{\rm D/H}]_{\rm ISM} \approx 2 \times 10^{-5}$, this implies that interstellar PAHs are D enriched by a factor of $[{\rm D/H}]_{\rm PAH}/[{\rm D/H}]_{\rm ISM} \approx 1200$.

We thank B.T. Draine and the anonymous referees for very helpful suggestions. X.J.Y. is supported in part by NSFC 11873041, 11473023 and the NSFC-CAS Joint Research Funds in Astronomy (U1731106, U1731107). A.L. is supported in part by NASA grants 80NSSC19K0572 and 80NSSC19K0701. R.G. is supported in part by the NSF-PRISM grant Mathematics and Life Sciences (0928053). Computations were performed using the high-performance computer resources of the University of Missouri Bioinformatics Consortium.

References

Allamandola, L. J., Hudgins, D. M., & Sandford, S. A. 1999, ApJ, 511, 115
Allamandola, L. J., Sandford, S. A., & Wopenka, B. 1987, Sci, 237, 56
Allamandola, L. J., Tielens, A. G. G. M., & Barker, J. R. 1985, ApJ, 290, L25
Allamandola, L. J., Tielens, A. G. G. M., & Barker, J. R. 1989, ApJS, 71, 733

[12] It is not clear whether or to what extent the strength and frequency of the aromatic C–D stretch would be affected when a deuterated PAH molecule is also attached by D-substituted aliphatic side groups (e.g., $-CH_2D$), or when some of its peripheral C atoms have one H atom and one extra D atom. Deuterated PAHs with D-substituted aliphatic side groups or excess D atoms are expected to exhibit both aromatic and aliphatic C–D stretches as seen in the ISO/SWS and AKARI spectra of the Orion Bar, M17, and H II regions (Peeters et al. 2004; Doney et al. 2016). It would be interesting to experimentally and computationally explore the frequencies and strengths of the aromatic and aliphatic C–H and C–D bands of such molecules. On the other hand, the aromatic C–D band at 4.4 μm and the aliphatic C–D band at ∼4.65–4.8 μm seen in the Orion Bar, M17, and H II regions may not necessarily be emitted by the same molecule (i.e., the former could be emitted by deuterated PAHs while the latter is emitted by PAHs attached by D-substituted aliphatic side groups or excess D atoms).

Bauschlicher, C. W., Langhoff, S. R., Sandford, S. A., & Hudgins, D. M. 1997, JPCA, 101, 2414
Bernstein, L. S., Shroll, R. M., Lynch, D. K., & Clark, F. O. 2017, ApJ, 836, 229
Bernstein, M. P., Sandford, S. A., & Allamandola, L. J. 1996, ApJ, 472, L127
Boesgaard, A. M., & Steigman, G. 1985, ARA&A, 23, 319
Borowski, P. 2012, JPCA, 116, 3866
Buragohain, M., Pathak, A., Sakon, I., & Onaka, T. 2020, ApJ, 892, 11
Buragohain, M., Pathak, A., Sarre, P., Onaka, T., & Sakon, I. 2015, MNRAS, 454, 193
Buragohain, M., Pathak, A., Sarre, P., Onaka, T., & Sakon, I. 2016, P&SS, 133, 97
Burles, S., Nollett, K. M., & Turner, M. S. 2001, ApJ, 552, L1
Coc, A., Vangioni-Flam, E., Descouvemont, P., Adahchour, A., & Angulo, C. 2004, ApJ, 600, 544
Cooke, R., Pettini, M., & Steidel, C. C. 2018, ApJ, 855, 102
Doney, K. D., Candian, A., Mori, T., Onaka, T., & Tielens, A. G. G. M. 2016, A&A, 586, 65
Draine, B. T. 2004, in Origin and Evolution of the Elements, ed. A. McWilliam & M. Rauch (Cambridge: Cambridge Univ. Press), 317
Draine, B. T. 2006, in ASP Conf. Ser. 348, Astrophysics in the Far Ultraviolet: Five Years of Discovery with FUSE, ed. G. Sonneborn, H. Moos, & B.-G. Andersson (San Francisco, CA: ASP), 58
Draine, B. T., & Li, A. 2001, ApJ, 551, 807
Draine, B. T., & Li, A. 2007, ApJ, 657, 810
Epstein, R. I., Lattimer, J. M., & Schramm, D. N. 1976, Natur, 263, 198
Frisch, M. J., Trucks, G. W., Schlegel, H. B., et al. 2009, Gaussian 09, Revision B01 (Wallingford, CT: Gaussian, Inc.)
Geballe, T. R., Lacy, J. H., Persson, S. E., McGregor, P. J., & Soifer, B. T. 1985, ApJ, 292, 500
Hébrard, G., Tripp, T. M., Chayer, P., et al. 2005, ApJ, 635, 1136
Hudgins, D. M., Bauschlicher, C. W., Jr., & Sandford, S. A. 2004, ApJ, 614, 770
Hudgins, D. M., Sandford, S. A., & Allamandola, L. J. 1994, JPhCh, 98, 4243
Jura, M. 1982, in Advances in UV Astronomy, Four Years of IUE Research, ed. Y. Kondo, J. M. Mead, & R. D. Chapman (Greenbelt, MD: NASA), 54
Kwok, S., & Zhang, Y. 2011, Natur, 479, 80
Li, A. 2009, in Small Bodies in Planetary Sciences, ed. I. Mann, A. Nakamura, & T. Mukai (Berlin: Springer), 167
Li, A. 2020, NatAs, 4, 339
Li, A., & Draine, B. T. 2012, ApJ, 760, L35
Linsky, J. L., Draine, B. T., Moos, H. W., et al. 2006, ApJ, 647, 1106
Mazzitelli, I., & Moretti, M. 1980, ApJ, 235, 995
Moos, H. W., Sembach, K. R., Vidal-Madjar, A., et al. 2002, ApJS, 140, 3
Onaka, T., Mori, T. I., Sakon, I., et al. 2014, ApJ, 780, 114
Peeters, E., Allamandola, L. J., Bauschlicher, C. W., Jr., et al. 2004, ApJ, 604, 252
Prodanović, T., Steigman, G., & Fields, B. D. 2010, MNRAS, 406, 1108
Sánchez, Ariel G., Baugh, C. M., Percival, W. J., et al. 2006, MNRAS, 366, 189
Sandford, S. A. 1991, ApJ, 376, 599
Sandford, S. A., Allamandola, L. J., Tielens, A. G. G. M., et al. 1991, ApJ, 371, 607
Sandford, S. A., Bernstein, M. P., & Dworkin, J. P. 2001, M&PS, 36, 1117
Sandford, S. A., Bernstein, M. P., & Materese, C. K. 2013, ApJS, 205, 8
Spergel, D. N., Verde, L., Peiris, H. V., et al. 2003, ApJS, 148, 175
Steigman, G. 2003, ApJ, 586, 1120
Verstraete, L., Puget, J. L., Falgarone, E., et al. 1996, A&A, 315, L337
Wiersma, S. D., Candian, A., Bakker, J. M., et al. 2020, A&A, 635, A9
Wood, B. E., Linsky, J. L., Hébrard, G., et al. 2004, ApJ, 609, 838
Yang, X. J., Glaser, R., Li, A., & Zhong, J. X. 2013, ApJ, 776, 110
Yang, X. J., Glaser, R., Li, A., & Zhong, J. X. 2017, NewAR, 77, 1
Yang, X. J., Li, A., & Glaser, R. 2020, ApJS, 247, 1
Zavarygin, E. O., Webb, J. K., Riemer-Sørensen, S., & Dumont, V. 2018, MNRAS, 477, 5536